Mutual Information Optimization for SIM-Based Holographic MIMO Systems

Nemanja Stefan Perović, *Member, IEEE* and Le-Nam Tran, *Senior Member, IEEE*

***Abstract*—In the context of emerging stacked intelligent metasurface (SIM)-based holographic MIMO (HMIMO) systems, a fundamental problem is to study the mutual information (MI) between transmitted and received signals to establish their capacity. However, direct optimization or analytical evaluation of the MI, particularly for discrete signaling, is often intractable. To address this challenge, we adopt the channel cutoff rate (CR) as an alternative optimization metric for the MI maximization. In this regard, we propose an alternating projected gradient method (APGM), which optimizes the CR of a SIM-based HMIMO system by adjusting signal precoding and the phase shifts across the transmit and receive SIMs in a layer-by-layer basis. Simulation results indicate that the proposed algorithm significantly enhances the CR, achieving substantial gains proportional to those observed for the corresponding MI. This justifies the effectiveness of using the channel CR for the MI optimization. Moreover, we demonstrate that the integration of digital precoding, even on a modest scale, has a significant impact on the ultimate performance of SIM-aided systems.**

***Index Terms*—Channel cutoff rate (CR), mutual information (MI), stacked intelligent metasurface (SIM), holographic MIMO (HMIMO), optimization.**

I. Introduction

Intelligent metasurfaces are expected to play a significant role in the evolution of future wireless communications. They are engineered surfaces, composed of a large number of controllable metamaterial elements that are capable of modifying the propagation of incident waves at the electromagnetic (EM) field level in dynamic and programmable manner [1]. This unique ability enables intelligent surfaces to improve energy efficiency, network capacity and connectivity, while also supporting other heterogeneous functions, such as localization and sensing. However, leveraging these advantages requires the acquisition of accurate channel state information (CSI), which presents a challenging task for conventional metasurface structures, such as reconfigurable intelligent surfaces (RISs). Furthermore, the multiplicative effect of the path loss of the RIS-assisted link severely reduces the possible gains through metasurface deployment. As a result, to maximize their potential, intelligent metasurfaces (e.g., RISs) are preferably placed in the vicinity of the transmitter and the receiver.

The above discussions naturally motivate the integration of intelligent metasurface structures with wireless communication transceivers in massive MIMO (mMIMO) and holographic MIMO (HMIMO) systems [2]. The use of intelligent metasurfaces in these systems offers a tradeoff between minimizing the number of radio frequency chains and maximizing the controllability over the radiated and received electromagnetic fields in the wave domain [3]. Moreover, the intelligent metasurfaces can provide beamforming capabilities comparable to those of conventional phased array antennas, but with much lower power consumption and cost. However, these metasurfaces are usually single-layer structures, which may limit their beamforming potential. In practical realizations, the elements of intelligent metasurfaces are constrained to a finite set of tunable states, and the number of these elements on a single metasurface is also limited. This can lead to beam misalignment, thereby undermining the expected performance results.

To address the above limitations, multi-layer metasurface structures have emerged as a promising solution for flexibly forming different radiation patterns compared to their single-layer counterparts. Such structures, called stacked intelligent metasurfaces (SIMs), were recently introduced [4], which is inspired from the architecture of a deep neural network [5]. Indeed, SIMs mirrors the multi-layer structure of neural networks that are, if properly trained, capable of modeling various functions with improved signal processing capabilities. In the same way, when metasurface layers are properly placed, SIM can implement signal processing directly in the EM wave domain. This approach can potentially reduce the reliance on digital beamforming and high-precision digital-to-analog converters.

In [6], the signal processing capabilities of SIMs were exploited for the implementation of 2D discrete Fourier transform (DFT) for direction of arrival (DOA) estimation. Moreover, a hybrid channel estimator, in which the received training symbols were processed first in the wave domain and later in the digital domain, was proposed in [7]. A general path loss model for an SIM-assisted wireless communication system was developed in [8], based on which, an algorithm for the receive power maximization was derived. In [9], the authors studied the achievable sum-rate maximization for a downlink channel between a SIM-assisted base station and multiple single-antenna users. Integrating SIMs with transmitters and receivers into the so-called SIM-based HMIMO system, which performs signal precoding and combining in the wave domain, was proposed in [10]. The introduced channel fitting approach enables the SIM-based HMIMO system to achieve significant channel capacity gains compared to mMIMO and RIS-assisted counterparts. Furthermore, the achievable rate optimization for the SIM-based HMIMO system was studied in [11].

Despite quite a few papers about SIM-based systems, none of them has considered the achievable rate of such systems using discrete signaling, i.e., the mutual information (MI). This gap has motivated us to investigate the optimization of the MI in the aforementioned systems. Since the direct optimization of the MI is intractable, we instead propose the use of the channel cutoff rate (CR) as an alternative metric to facilitate the MI optimization [12], [13]. The channel CR can be seen as a lower bound on the MI [12, Eq. (36)] and is widely recognized as a practical upper limit on the information rate that guarantees reliable communications.

The main contributions of this paper are listed as follows:

- We show that using the channel CR as an alternative optimization metric enables efficient maximization of the MI in SIM-based HMIMO systems. Specifically, the CR is expressed as a closed-form expression, which facilitates the derivation of efficient optimization algorithms.
- To maximize the CR, we formulate a joint optimization problem of transmit precoding and the phase shifts for both transmit and receive SIMs. Then an alternating projected gradient method (APGM) is proposed to solve this problem, which particularly optimizes the phase shifts for the transmit and receive SIMs in a layer-by-layer basis. Moreover, we provide the computational complexity of the proposed algorithm.
- We demonstrate through simulation results that the proposed algorithm can significantly increase the CR and the MI in a proportional manner. Also, the increase of the modulation order without changing the transmit signal power has a negligible influence on the MI. Finally, incorporating even a small scale digital precoding into a SIM-based HMIMO system leads to substantial improvements on the achievable MI.

II. System Model

We consider a SIM-based HMIMO communication system with N_t transmit antennas and N_r receive antennas, where both the transmitter and the receiver are equipped with SIMs. The transmit SIM consists of L metasurface layers with N meta-atoms in each layer, while the receive SIM consists of K metasurface layers with E meta-atoms in each layer. The meta-atoms of the SIMs are connected to smart controllers or field programmable gate array (FPGA) devices, which can independently adjust the phase shift of each meta-atom. In this way, MIMO transceivers with closely spaced SIMs can implement signal beamforming directly in the EM wave domain.

For the l-th layer of the transmit SIM, the phase shift matrix is denoted as $\mathbf{\Phi}^l = \text{diag}(\boldsymbol{\phi}^l) = \text{diag}([\phi_1^l \, \phi_2^l \, \cdots \, \phi_N^l]^T)$, where diag$(\cdot)$ transforms a vector into a diagonal matrix. Also, $\phi_n^l = \exp(j\theta_n^l)$, where θ_n^l is the phase shift of the n-th meta-atom in the l-th layer. Signal propagation between the $(l-1)$-th and l-th layer of the transmit SIM is modeled by the matrix $\mathbf{W}^l \in \mathbb{C}^{N\times N}$, where $[\mathbf{W}^l]_{m,n}$ denotes the signal propagation between the n-th meta-atom of the $(l-1)$-th layer and the m-th meta-atom of the l-th layer. According to Rayleigh-Sommerfeld diffraction theory, $[\mathbf{W}^l]_{m,n}$ is given by [14, Eq. (1)]

$$[\mathbf{W}^l]_{m,n} = \frac{A\cos\chi_{m,n}}{d_{m,n}}\Big(\frac{1}{2\pi d_{m,n}} - \frac{j}{\lambda}\Big)e^{j\frac{2\pi d_{m,n}}{\lambda}} \tag{1}$$

for $l = 2, 3, \ldots, L$, where A is the area of each meta-atom, $d_{m,n}$ is the propagation distance between the meta-atoms in the $(l-1)$-th and l-th layer of the transmit SIM, $\chi_{m,n}$ is the angle between the propagation direction and normal direction of the $(l-1)$-th layer[1]. Similarly, signal propagation between the transmit antenna array and the first layer of the transmit SIM is modeled by $\mathbf{W}^1 \in \mathbb{C}^{N\times N_t}$, which is defined as (1). Finally, the EM wave domain beamforming matrix of the transmit SIM can be written as

$$\mathbf{B} = \mathbf{\Phi}^L\mathbf{W}^L \cdots \mathbf{\Phi}^2\mathbf{W}^2\mathbf{\Phi}^1\mathbf{W}^1 \in \mathbb{C}^{N\times N_t}. \tag{2}$$

At the receive SIM, the phase shift matrix for the k-th layer is given by $\mathbf{\Psi}^k = \text{diag}(\boldsymbol{\psi}^k) = \text{diag}([\psi_1^k \, \psi_2^k \, \cdots \, \psi_E^k]^T)$, where $\psi_e^k = \exp(j\upsilon_e^k)$ and υ_e^k is the phase shift of the e-th meta-atom in the k-th layer. Signal propagation between the k-th and $(k-1)$-th layer of the receive SIM is modeled by the matrix $\mathbf{U}^k \in \mathbb{C}^{E\times E}$, which is defined similarly as in (1). Also, signal propagation between the first layer of the receive SIM and the receive antenna array is given by $\mathbf{U}^1 \in \mathbb{C}^{N_r\times E}$. The EM wave domain beamforming matrix for the receive SIM can be expressed as

$$\mathbf{Z} = \mathbf{U}^1\mathbf{\Psi}^1\mathbf{U}^2\mathbf{\Psi}^2 \cdots \mathbf{U}^K\mathbf{\Psi}^K \in \mathbb{C}^{N_r\times E}. \tag{3}$$

Let $\mathbf{G}$ be the channel between the transmit and the receive SIM. Then the end-to-end channel matrix for the considered communication system is written as

$$\mathbf{H} = \mathbf{ZGB} \in \mathbb{C}^{N_r\times N_t} \tag{4}$$

and the signal vector at the receive antennas is given by

$$\mathbf{y} = \mathbf{HP}\mathbf{x}_i + \mathbf{n} \tag{5}$$

where $\mathbf{P} \in \mathbb{C}^{N_t\times N_s}$ is the precoding matrix that satisfies the following the average transmit power constraint:

$$\text{Tr}(\mathbf{PP}^H) = N_s \tag{6}$$

where $N_s \le \min(N_t, N_r)$ is the number of the transmitted modulation symbols. The transmit vector $\mathbf{x}_i \in \mathbb{C}^{N_s\times 1}$ consists of elements chosen from a discrete symbol alphabet of size M, and thus, the number of different transmit vectors is $N_{vec} = M^{N_s}$. In addition, it is assumed that the average symbol energy of the discrete symbol alphabet is one. Finally, $\mathbf{n} \in \mathbb{C}^{N_r\times 1}$ is the noise vector with independent and identically distributed (i.i.d.) elements that are distributed according to $\mathcal{CN}(0, \sigma^2)$, where σ^2 is the noise variance.

III. Problem Formulation

We consider a discrete-input continuous-output memoryless channel (DCMC). For equally probable transmitted symbol vectors, the MI is found as [12], [13]

$$\text{MI} = \log_2(N_{vec}) - \frac{1}{N_{vec}}\sum_{i=1}^{N_{vec}}\mathbb{E}_{\mathbf{n}}\Big\{\log_2\sum_{j=1}^{N_{vec}} e^{\kappa_{i,j}}\Big\} \tag{7}$$

where $\kappa_{i,j} = (-||\mathbf{HP}(\mathbf{x}_i - \mathbf{x}_j) + \mathbf{n}||^2 + ||\mathbf{n}||^2)/\sigma^2$.

As the direct optimization of the MI in (7) involves discrete variables, which is intractable, we instead consider the optimization of a closed related metric, known as the CR, which is given by

$$R_0 = -\log_2\Big[\frac{1}{N_{vec}^2}\sum_{i,j=1}^{N_{vec}} e^{-\frac{F_{i,j}}{4\sigma^2}}\Big] \tag{8}$$

[1]In this paper, it is assumed that all layers of the transmit SIM have the same arrangement and thus the right-hand side (RHS) of (1) does not depend on l. The same applies for the receive SIM.

Algorithm 1: APGM algorithm for solving (9).

Input: $\mathbf{P}_0$, $\boldsymbol{\phi}_0$, $\boldsymbol{\psi}_0$, $\nu_0 > 0$, $\mu_0^{1:L} > 0$, $\tau_0^{1:K} > 0$, $n \leftarrow 0$, $0 < \rho < 1$, $\delta > 0$.

1 **repeat**
2   **repeat** /* line search for $\mathbf{P}$ */
3         $\mathbf{P}_{n+1} = \mathcal{P}_P(\mathbf{P}_n - \nu_n \nabla_{\mathbf{P}} f(\mathbf{P}_n, \boldsymbol{\phi}_n, \boldsymbol{\psi}_n))$
4   **if** $f(\mathbf{P}_{n+1}, \boldsymbol{\phi}_n, \boldsymbol{\psi}_n) > f(\mathbf{P}_n, \boldsymbol{\phi}_n, \boldsymbol{\psi}_n) - \delta \|\mathbf{P}_{n+1} - \mathbf{P}_n\|^2$ **then**
5             $\nu_n \leftarrow \rho \nu_n$
6   **end**
7   **until** $f(\mathbf{P}_{n+1}, \boldsymbol{\phi}_n, \boldsymbol{\psi}_n) \le f(\mathbf{P}_n, \boldsymbol{\phi}_n, \boldsymbol{\psi}_n) - \delta \|\mathbf{P}_{n+1} - \mathbf{P}_n\|^2$
8   **for** $l = 1$ **to** L **do**
9   **repeat** /* line search for $\boldsymbol{\phi}^l$ */
10             $\boldsymbol{\phi}_{n+1}^l = \mathcal{P}_\phi(\boldsymbol{\phi}_n^l - \mu_n^l \nabla_{\boldsymbol{\phi}^l} f(\mathbf{P}_{n+1}, \bar{\boldsymbol{\phi}}_n^l, \boldsymbol{\psi}_n))$
11   **if** $f(\mathbf{P}_{n+1}, \bar{\boldsymbol{\phi}}_{n+1}^l, \boldsymbol{\psi}_n) > f(\mathbf{P}_{n+1}, \bar{\boldsymbol{\phi}}_n^l, \boldsymbol{\psi}_n) - \delta \|\boldsymbol{\phi}_{n+1}^l - \boldsymbol{\phi}_n^l\|^2$ **then**
12                 $\mu_n^l \leftarrow \rho \mu_n^l$
13   **end**
14   **until** $f(\mathbf{P}_{n+1}, \bar{\boldsymbol{\phi}}_{n+1}^l, \boldsymbol{\psi}_n) \le f(\mathbf{P}_{n+1}, \bar{\boldsymbol{\phi}}_n^l, \boldsymbol{\psi}_n) - \delta \|\boldsymbol{\phi}_{n+1}^l - \boldsymbol{\phi}_n^l\|^2$
15   **end**
16   **for** $k = 1$ **to** K **do**
17   **repeat** /* line search for $\boldsymbol{\psi}^k$ */
18             $\boldsymbol{\psi}_{n+1}^k = \mathcal{P}_{\boldsymbol{\psi}}(\boldsymbol{\psi}_n^k - \tau_n^k \nabla_{\boldsymbol{\psi}^k}(\mathbf{P}_{n+1}, \boldsymbol{\phi}_{n+1}, \bar{\boldsymbol{\psi}}_n^k)$
19   **if** $f(\mathbf{P}_{n+1}, \boldsymbol{\phi}_{n+1}, \bar{\boldsymbol{\psi}}_{n+1}^k) > f(\mathbf{P}_{n+1}, \boldsymbol{\phi}_{n+1}, \bar{\boldsymbol{\psi}}_n^k) - \delta \|\boldsymbol{\psi}_{n+1}^k - \boldsymbol{\psi}_n^k\|^2$ **then**
20                 $\tau_n^k \leftarrow \rho \tau_n^k$
21   **end**
22   **until** $f(\mathbf{P}_{n+1}, \boldsymbol{\phi}_{n+1}, \bar{\boldsymbol{\psi}}_{n+1}^k) \le f(\mathbf{P}_{n+1}, \boldsymbol{\phi}_{n+1}, \bar{\boldsymbol{\psi}}_n^k) - \delta \|\boldsymbol{\psi}_{n+1}^k - \boldsymbol{\psi}_n^k\|^2$
23   **end**
24     $n \leftarrow n + 1$
25 **until** *convergence*

where $F_{i,j} = ||\mathbf{H}\mathbf{P}(\mathbf{x}_i - \mathbf{x}_j)||^2 = ||\mathbf{H}\mathbf{P}\Delta\mathbf{x}_{i,j}||^2$. Since the CR decreases with the argument of the logarithm function in (8), maximizing R_0 is equivalent to the following optimization problem [13]

$$\underset{\mathbf{P}, \boldsymbol{\phi}, \boldsymbol{\psi}}{\text{minimize}} \ f(\mathbf{P}, \boldsymbol{\phi}, \boldsymbol{\psi}) = \sum\nolimits_{i,j=1}^{N_{vec}} e^{-\frac{F_{i,j}}{4\sigma^2}} \tag{9a}$$

$$\text{subject to} \ \ |\boldsymbol{\phi}| = 1, \tag{9b}$$

$$|\boldsymbol{\psi}| = 1, \tag{9c}$$

$$\text{Tr}(\mathbf{P}\mathbf{P}^H) = N_s, \tag{9d}$$

where $\boldsymbol{\phi} = [(\boldsymbol{\phi}^1)^T, (\boldsymbol{\phi}^2)^T, \ldots, (\boldsymbol{\phi}^L)^T]^T \in \mathbb{C}^{(NL)\times 1}$, $\boldsymbol{\psi} = [(\boldsymbol{\psi}^1)^T, (\boldsymbol{\psi}^2)^T, \ldots, (\boldsymbol{\psi}^K)^T]^T \in \mathbb{C}^{(MK)\times 1}$, and the equalities in (9b) and (9c) are treated element-wise.

IV. Proposed Optimization Method

We remark that (9) can potentially become a large-scale optimization problem, and thus, first order methods are particularly suitable. Indeed, we adopt the APGM to derive the proposed method for solving (9), which is summarized in **Algorithm 1**. Let $(\mathbf{P}_n, \boldsymbol{\phi}_n, \boldsymbol{\psi}_n)$ be the value of $(\mathbf{P}, \boldsymbol{\phi}, \boldsymbol{\psi})$ at iteration n. Then $\mathbf{P}_{n+1}$ is obtained as

$$\mathbf{P}_{n+1} = \mathcal{P}_P(\mathbf{P}_n - \nu_n \nabla_{\mathbf{P}} f(\mathbf{P}_n, \boldsymbol{\phi}_n, \boldsymbol{\psi}_n)) \tag{10}$$

where $\nabla_{\mathbf{P}} f(\mathbf{P}, \boldsymbol{\phi}, \boldsymbol{\psi})$ is the gradient of $f(\mathbf{P}, \boldsymbol{\phi}, \boldsymbol{\psi})$ with respect to (w.r.t.) $\mathbf{P}^*$, $\mathcal{P}_P(\cdot)$ denotes the projection onto the set defined by (6) and ν_n is the step size, which is found by the line search routine described in steps **2** to **7** of **Algorithm 1**.

In optimizing the phase shifts of the SIMs, existing algorithms typically perform a projected gradient step across all phase shifts of all layers simultaneously using the same step size [6], [7]. However, we have observed that such a method results in a poor performance. To address this, our proposed algorithm optimizes the phase shifts for the transmit and the receive SIMs in a layer-by-layer basis, with each layer being assigned a separate step size. This approach is shown to yield better performance results in our numerical experiments.

More specifically, the phase shifts of the l-th layer of the transmit SIM at iteration $n+1$ is determined by

$$\boldsymbol{\phi}_{n+1}^l = \mathcal{P}_{\boldsymbol{\phi}^l}(\boldsymbol{\phi}_n^l - \mu_n^l \nabla_{\boldsymbol{\phi}^l} f(\mathbf{P}_{n+1}, \bar{\boldsymbol{\phi}}_n^l, \boldsymbol{\psi}_n)) \tag{11}$$

for $l = 1, 2, \ldots, L$, and where we denote $\bar{\boldsymbol{\phi}}_n^l = [(\boldsymbol{\phi}_{n+1}^1)^T, \ldots, (\boldsymbol{\phi}_{n+1}^{l-1})^T, (\boldsymbol{\phi}_n^l)^T, \ldots, (\boldsymbol{\phi}_n^L)^T]^T$ and $\bar{\boldsymbol{\phi}}_{n+1}^l = [(\boldsymbol{\phi}_{n+1}^1)^T, \ldots, (\boldsymbol{\phi}_{n+1}^l)^T, (\boldsymbol{\phi}_n^{l+1})^T, \ldots, (\boldsymbol{\phi}_n^L)^T]^T$. In the above, $\nabla_{\boldsymbol{\phi}^l} f(\mathbf{P}, \boldsymbol{\phi}, \boldsymbol{\psi})$ is the gradient of $f(\mathbf{P}, \boldsymbol{\phi}, \boldsymbol{\psi})$ w.r.t. $\boldsymbol{\phi}^{l*}$, $\mathcal{P}_{\boldsymbol{\phi}^l}(\cdot)$ denotes the projection onto (9b), and μ_n^l is the step size for the l-th layer. The line search procedure for finding μ_n^l is outlined in steps **9** to **14**. Similarly, $\boldsymbol{\psi}_{n+1}^k$ is found as

$$\boldsymbol{\psi}_{n+1}^k = \mathcal{P}_{\boldsymbol{\psi}^k}(\boldsymbol{\psi}_n^k - \tau_n^k \nabla_{\boldsymbol{\psi}^k} f(\mathbf{P}_{n+1}, \boldsymbol{\phi}_{n+1}, \bar{\boldsymbol{\psi}}_n^k)), \tag{12}$$

where $\nabla_{\boldsymbol{\psi}^k} f(\mathbf{P}, \boldsymbol{\phi}, \boldsymbol{\psi})$ is the gradient of $f(\mathbf{P}, \boldsymbol{\phi}, \boldsymbol{\psi})$ w.r.t. $\boldsymbol{\psi}^{k*}$, and τ_n^k is the step size, which is determined in steps **17** to **22**. The involved gradients are provided in **Theorem 1**.

Theorem 1. *The gradients of $f(\mathbf{P}, \boldsymbol{\phi}, \boldsymbol{\psi})$ with respect to $\mathbf{P}^*$, $\boldsymbol{\phi}^{l*}$ and $\boldsymbol{\psi}^{k*}$ are given by*

$$\nabla_{\mathbf{P}} f(\mathbf{P}, \boldsymbol{\phi}, \boldsymbol{\psi}) = -\frac{1}{4\sigma^2} \mathbf{H}^H \mathbf{H}\mathbf{P} \sum_{i,j=1}^{N_{vec}} e^{-\frac{F_{i,j}}{4\sigma^2}} \Delta\mathbf{x}_{i,j} \Delta\mathbf{x}_{i,j}^H \tag{13}$$

$$\nabla_{\boldsymbol{\phi}^l} f(\mathbf{P}, \boldsymbol{\phi}, \boldsymbol{\psi}) = -\frac{1}{4\sigma^2} \sum_{i,j=1}^{N_{vec}} e^{-\frac{F_{i,j}}{4\sigma^2}} \operatorname{vec}_d(\mathbf{L}_l) \tag{14}$$

$$\nabla_{\boldsymbol{\psi}^k} f(\mathbf{P}, \boldsymbol{\phi}, \boldsymbol{\psi}) = -\frac{1}{4\sigma^2} \sum_{i,j=1}^{N_{vec}} e^{-\frac{F_{i,j}}{4\sigma^2}} \operatorname{vec}_d(\mathbf{K}_k) \tag{15}$$

where

$$\mathbf{L}_l = \boldsymbol{\Theta}^{l+1:L} \mathbf{G}^H \mathbf{Z}^H \mathbf{H}\mathbf{P} \Delta\mathbf{x}_{i,j} \Delta\mathbf{x}_{i,j}^H \mathbf{P}^H \boldsymbol{\Theta}^{1:l-1} (\mathbf{W}^l)^H \tag{16a}$$

$$\mathbf{K}_k = (\mathbf{U}^k)^H \boldsymbol{\Upsilon}^{k-1:1} \mathbf{H}\mathbf{P} \Delta\mathbf{x}_{i,j} \Delta\mathbf{x}_{i,j}^H \mathbf{P}^H \mathbf{B}^H \mathbf{G}^H \boldsymbol{\Upsilon}^{K:k+1} \tag{16b}$$

where $\boldsymbol{\Theta}^{m:n} = (\mathbf{W}^m)^H (\boldsymbol{\Phi}^m)^H \cdots (\mathbf{W}^n)^H (\boldsymbol{\Phi}^n)^H$ *and* $\boldsymbol{\Upsilon}^{m:n} = (\boldsymbol{\Psi}^m)^H (\mathbf{U}^m)^H \cdots (\boldsymbol{\Psi}^m)^H (\mathbf{U}^n)^H$.

Proof: See the Appendix. ■

After calculating the gradients, the next step is to perform projection onto the corresponding feasible sets. It is easy to see from (6) that $\mathcal{P}_P(\mathbf{P})$ is given by

$$\overline{\mathbf{P}} = \mathbf{P}\sqrt{N_s / \operatorname{Tr}(\mathbf{P}\mathbf{P}^H)}. \tag{17}$$

Since the elements of $\boldsymbol{\phi}^l$ are constrained to lie on the unit circle, $\mathcal{P}_\phi(\boldsymbol{\phi}^l)$ is defined by

$$\overline{\phi_n^l} = \begin{cases} \phi_n^l / |\phi_n^l|, & \phi_n^l \neq 0 \\ \exp(j\alpha), \alpha \in [0, 2\pi] & \phi_n^l = 0. \end{cases} \tag{18}$$

For $\phi_n^l = 0$, the projection can take any point on the unit circle. Finally, $\mathcal{P}_{\boldsymbol{\psi}}(\boldsymbol{\psi}^k)$ is obtained similarly as in (18).

V. Computational Complexity

In this section, the computational complexity of **Algorithm 1** is analyzed by counting the required number of complex multiplications. We assume that $N \gg N_t$ and $E \gg N_r$, which is the usual case for a SIM-based HMIMO communication system. We also assume that all matrices $\triangle\mathbf{x}_{i,j}\triangle\mathbf{x}_{i,j}^H$ are precomputed. In the sequel, we provide the complexity for the computation of the precoding matrix $\mathbf{P}$, and the transmit and the receive SIM phase shifts $\{\boldsymbol{\phi}^l\}_{l=1}^L$ and $\{\boldsymbol{\psi}^k\}_{k=1}^K$, respectively.

The complexity of calculating all products $e^{-\frac{F_{i,j}}{4\sigma^2}}\triangle\mathbf{x}_{i,j}\triangle\mathbf{x}_{i,j}^H$ in (13) is $\mathcal{O}(N_{vec}^2 N_s^2)$, this is also the complexity of calculating the gradient $\nabla_{\mathbf{P}} f(\mathbf{P}, \boldsymbol{\phi}, \boldsymbol{\psi})$. In addition, $\mathcal{O}(N_{vec}^2 N_s^2)$ multiplications are required to obtain $f(\mathbf{P}_{n+1}, \boldsymbol{\phi}_n, \boldsymbol{\psi}_n)$. Hence, the complexity of computing the precoding matrix $\mathbf{P}$ is equal to $\mathcal{O}(I_p N_{vec}^2 N_s^2)$, where I_p is the number of line search steps.

The complexity of $\sum_{i,j} e^{-\frac{F_{i,j}}{4\sigma^2}}\triangle\mathbf{x}_{i,j}\triangle\mathbf{x}_{i,j}^H$ in (14) is $\mathcal{O}(N_{vec}^2 N_s^2)$. The complexity of calculating the matrix product $\mathbf{G}^H\mathbf{Z}^H\mathbf{H}\mathbf{P}\sum_{i,j} e^{-\frac{F_{i,j}}{4\sigma^2}}\triangle\mathbf{x}_{i,j}\triangle\mathbf{x}_{i,j}^H\mathbf{P}^H$ can be neglected. Furthermore, $\mathcal{O}(LN^3)$ multiplications are needed to calculate $\mathbf{L}_l$. Hence, the complexity of calculating the gradient $\nabla_{\boldsymbol{\phi}^l} f(\mathbf{P}, \boldsymbol{\phi}, \boldsymbol{\psi})$ is $\mathcal{O}(N_{vec}^2 N_s^2 + LN^3)$. After obtaining $\boldsymbol{\phi}_{n+1}^l$, the calculation of $\mathbf{B}$ has the complexity of $\mathcal{O}(LN^3)$ and $\mathcal{O}(MN\min(N_t, N_r))$ multiplications are required to compute $\mathbf{H}$. The complexity of calculating $f(\mathbf{P}_{n+1}, \bar{\boldsymbol{\phi}}_{n+1}^l, \boldsymbol{\psi}_n)$ is $\mathcal{O}(N_{vec}^2 N_s^2)$. Therefore, the complexity of computing the transmit SIM phase shifts $\{\boldsymbol{\phi}^l\}_{l=1}^L$ is given by $\mathcal{O}(L[N_{vec}^2 N_s^2 + LN^3 + I_{\boldsymbol{\phi}}(LN^3 + MN\min(N_t, N_r) + N_{vec}^2 N_s^2)])$, where $I_{\boldsymbol{\phi}}$ is the number of line search loops. In a similar way, the complexity of computing the receive SIM phase shifts $\{\boldsymbol{\psi}^k\}_{k=1}^K$ is equal to $\mathcal{O}(K[N_{vec}^2 N_s^2 + KE^3 + I_{\boldsymbol{\psi}}(KE^3 + EN\min(N_t, N_r) + N_{vec}^2 N_s^2)])$, where $I_{\boldsymbol{\psi}}$ is the number of line search steps.

In summary, the complexity of one iteration of the APGM algorithm is given by

$$\begin{aligned} C_{\text{APGM}} = \mathcal{O}(&I_p N_{vec}^2 N_s^2 + L[N_{vec}^2 N_s^2 + LN^3 + I_{\boldsymbol{\phi}}(LN^3 + \\ &MN\min(N_t, N_r) + N_{vec}^2 N_s^2)] + K[N_{vec}^2 N_s^2 + KE^3 \\ &+ I_{\boldsymbol{\psi}}(KE^3 + EN\min(N_t, N_r) + N_{vec}^2 N_s^2)]). \end{aligned} \tag{19}$$

VI. Simulation Results

In this section, we evaluate the CR and the MI of **Algorithm 1** in a SIM-based HMIMO setup. The channel matrix between the transmit and the receive SIM is modeled based on the spatially-correlated channel model as $\mathbf{G} = \mathbf{R}_{\text{R}}^{1/2}\bar{\mathbf{G}}\mathbf{R}_{\text{T}}^{1/2} \in \mathbb{C}^{E\times L}$ [10], [11] where $\bar{\mathbf{G}} \in \mathbb{C}^{E\times L}$ is distributed according to $\mathcal{CN}(0, \beta\mathbf{I})$; β is the free space path loss between the transmit and the receive SIM modeled as $\beta(d) = \beta(d_0) + 10b\log_{10}(d/d_0)$, where $\beta(d_0) = 20\log_{10}(4\pi d_0/\lambda)$ is the free space path loss at the reference distance d_0, b is the path loss exponent, and d is the distance between the transmitter and the receiver. Moreover, $\mathbf{R}_{\text{T}} \in \mathbb{C}^{L\times L}$ and $\mathbf{R}_{\text{R}} \in \mathbb{C}^{E\times E}$ are the spatial correlation matrices of the transmit and the receive SIM, respectively, and the elements of these matrices are given by [10, Eq. (14), (15)].

In the following simulation setup, the parameters are $\lambda = 5\,\text{cm}$ (i.e., $f = 6\,\text{GHz}$), $N_t = 2$, $N_r = 2$, $N_s = 2$, $\beta = 3.5$, $d_0 = 1\,\text{m}$, $d = 300\,\text{m}$, $L = K = 4$ and $\sigma^2 = -110\,\text{dB}$. Both the transmit and the receive antennas are placed in arrays parallel to the x-axis, and the midpoints of these arrays have coordinates $(0,0,0)$ and $(0,0,d)$, respectively. Also, the inter-antenna separations of these arrays are $\lambda/2$. The meta-atoms in every SIM layer are uniformly placed in a square formation and the size of each meta-atom is $\frac{\lambda}{2} \times \frac{\lambda}{2}$ (i.e., $A = \lambda^2/4$). Moreover, all SIM layers are parallel to the xy-plane and their centers are along the z-axis. The separation between the neighboring SIM layers, as well as the separation between the first SIM layer and the adjacent antenna array are $\lambda/2$. In the line search procedures in **Algorithm 1**, all step sizes are initially set to 1000, $\delta = 10^{-3}$ and $\rho = 1/2$. The initial values of the optimization variables $\mathbf{P}$, $\boldsymbol{\phi}$, and $\boldsymbol{\psi}$ are randomly generated. All results are averaged over 30 independent channel realizations.

In Fig. 1, we present the CR and the MI of the proposed APGM algorithm for different sizes of the discrete symbol alphabet and different numbers of meta-atoms in SIM layers. In general, the MI reflects the same trend as observed in the CR, albeit always achieving larger values. This justifies the use of the CR as an alternative metric for the MI optimization. In all cases, the CR and the MI reach 90 % of their convergent values in approximately 20 iterations of the proposed algorithm. Furthermore, we notice that the change of M has a negligible influence on the CR, and that the MI may even decrease slightly if M increases when the transmit and receive SIMs have 49 meta-atoms per layer. This phenomenon is due to the reduced separation between adjacent constellation points when M is increased without a corresponding increase in the average symbol energy, which consequently increases the bit error probability (BEP) per transmission interval. On the other hand, the CR and the MI demonstrate significant improvements as the number of meta-atoms in the SIM layers increases. This enhancement reaffirms the fact that the beamforming capabilities of SIMs are highly dependent on the number of meta-atoms in SIM layers.

In Fig. 2, we show the MI of the considered system with and without signal precoding. It can be clearly observed that signal precoding can substantially increase the MI for about 47 % and 32 % for 49 and 100 meta-atoms per SIM layer, respectively. On the other side, signal precoding alone, i.e., in the absence of the transmit and the receive SIMs, is only able to provide a near zero MI, which is not shown in Fig. 2. Hence, we can conclude that while digital signal precoding of small scale alone shows limited beamforming gain, but its integration with SIM-based HMIMO systems can generate significant impact on the achievable MI.

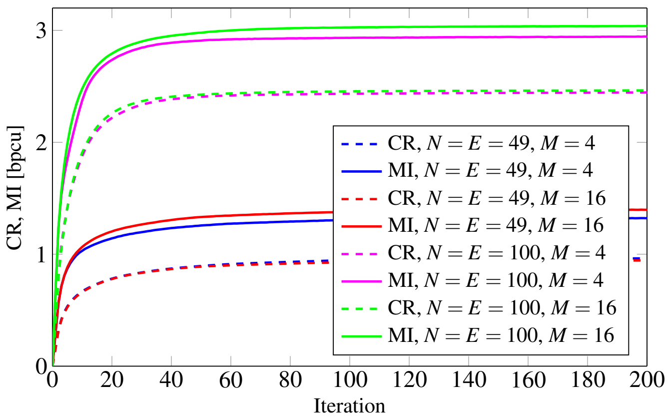

Fig. 1. CR and MI of the proposed APGM algorithm.

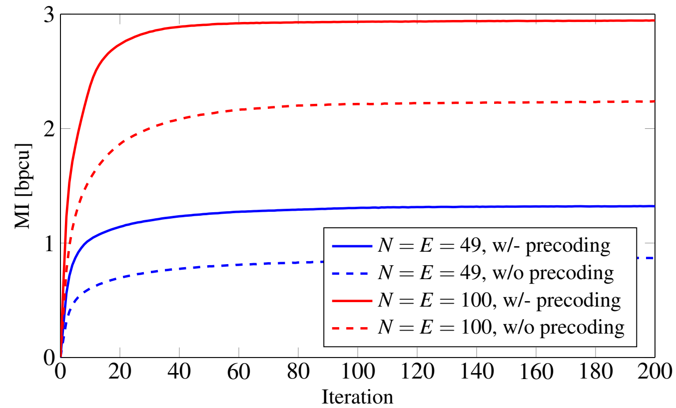

Fig. 2. MI of the considered system with (w/-) and without (w/o) signal precoding ($M = 4$).

VII. Conclusion

In this paper, we have demonstrated that the MI in a SIM-based HMIMO system can be efficiently optimized with the channel CR. To maximize the CR, we proposed the APGM which optimizes for the CR by adjusting the transmit precoding, and the phase shifts for the transmit and the receive SIMs in a layer-by-layer basis. Simulation results show that the CR is indeed a reliable metric for optimizing the MI in SIM-based HMIMO systems. Also, integrating even a small scale digital precoder in the considered system can substantially increase the MI performance.

Appendix
Proof of Theorem 1

The gradient of $f(\mathbf{P},\boldsymbol{\phi},\boldsymbol{\psi})$ with respect to $\mathbf{P}^*$ is given by

$$\nabla_{\mathbf{P}} f(\mathbf{P},\boldsymbol{\phi},\boldsymbol{\psi}) = -\frac{1}{4\sigma^2}\sum_{i,j=1}^{N_s}\exp\left(-\frac{F_{i,j}}{4\sigma^2}\right)\nabla_{\mathbf{P}} F_{i,j}. \quad (20)$$

Differentiating $F_{i,j}$, we obtain

$$\mathrm{d}F_{i,j} = \mathrm{Tr}\{(\mathbf{H}^H\mathbf{H}\mathbf{P}\Delta\mathbf{x}_{i,j}\Delta\mathbf{x}_{i,j}^H)^T\mathrm{d}\mathbf{P}^* + \Delta\mathbf{x}_{i,j}\Delta\mathbf{x}_{i,j}^H\mathbf{P}^H\mathbf{H}^H\mathbf{H}\mathrm{d}\mathbf{P}\}$$

which becomes clear that

$$\nabla_{\mathbf{P}} F_{i,j} = \mathbf{H}^H\mathbf{H}\mathbf{P}\Delta\mathbf{x}_{i,j}\Delta\mathbf{x}_{i,j}^H. \quad (21)$$

Substituting (21) into (20), we obtain (13).

The gradient of $f(\mathbf{P},\boldsymbol{\phi},\boldsymbol{\psi})$ with respect to $\boldsymbol{\phi}^{l*}$ is given by

$$\nabla_{\boldsymbol{\phi}^l} f(\mathbf{P},\boldsymbol{\phi},\boldsymbol{\psi}) = -\frac{1}{4\sigma^2}\sum_{i,j=1}^{N_s}\exp\left(-\frac{F_{i,j}}{4\sigma^2}\right)\nabla_{\boldsymbol{\phi}^l} F_{i,j}. \quad (22)$$

Differentiating again $F_{i,j}$ (but now w.r.t. $\boldsymbol{\phi}^l$) yields

$$\begin{aligned}\mathrm{d}F_{i,j} &= \mathrm{Tr}\{\mathbf{H}\mathbf{P}\Delta\mathbf{x}_{i,j}\Delta\mathbf{x}_{i,j}^H\mathbf{P}^H\mathrm{d}\mathbf{H}^H + \mathbf{P}\Delta\mathbf{x}_{i,j}\Delta\mathbf{x}_{i,j}^H\mathbf{P}^H\mathbf{H}^H\mathrm{d}\mathbf{H}\}\\ &= \mathrm{Tr}\{\mathbf{L}_l\mathrm{d}(\boldsymbol{\Phi}^l)^H + \mathbf{L}_l^H\mathrm{d}\boldsymbol{\Phi}^l\} = \mathrm{Tr}\{\mathbf{L}_l^T\mathrm{d}\boldsymbol{\Phi}^{l*} + \mathbf{L}_l^H\mathrm{d}\boldsymbol{\Phi}^l\}\\ &= \mathrm{vec}^T(\mathbf{L}_l)\,\mathrm{vec}(\boldsymbol{\Phi}^{l*}) + \mathrm{vec}^T(\mathbf{L}_l^*)\,\mathrm{vec}(\boldsymbol{\Phi}^l). \quad (23)\end{aligned}$$

Thus, we can conclude that

$$\nabla_{\boldsymbol{\phi}^l} F_{i,j} = \mathrm{vec}_d(\mathbf{L}_l), \quad (24)$$

and substituting this gradient into (22), we obtain (14). Following the same steps, we can also prove (15).

References

[1] M. Di Renzo *et al.*, "Smart radio environments empowered by reconfigurable intelligent surfaces: How it works, state of research, and the road ahead," *IEEE Journal on Selected Areas in Communications*, vol. 38, no. 11, pp. 2450–2525, 2020.

[2] N. Shlezinger *et al.*, "Dynamic metasurface antennas for 6G extreme massive MIMO communications," *IEEE Wireless Communications*, vol. 28, no. 2, pp. 106–113, 2021.

[3] M. Di Renzo and M. D. Migliore, "Electromagnetic signal and information theory," *IEEE BITS the Information Theory Magazine*, 2024, Early Access.

[4] J. An *et al.*, "Stacked intelligent metasurface-aided MIMO transceiver design," *arXiv preprint arXiv:2311.09814*, 2023.

[5] C. Liu *et al.*, "A programmable diffractive deep neural network based on a digital-coding metasurface array," *Nature Electronics*, vol. 5, no. 2, pp. 113–122, 2022.

[6] J. An *et al.*, "Two-dimensional direction-of-arrival estimation using stacked intelligent metasurfaces," *arXiv preprint arXiv:2402.08224*, 2024.

[7] Q.-U.-A. Nadeem *et al.*, "Hybrid digital-wave domain channel estimator for stacked intelligent metasurface enabled multi-user miso systems," *arXiv preprint arXiv:2309.16204*, 2023.

[8] N. U. Hassan *et al.*, "Efficient beamforming and radiation pattern control using stacked intelligent metasurfaces," *IEEE Open Journal of the Communications Society*, vol. 5, pp. 599–611, 2024.

[9] J. An *et al.*, "Stacked intelligent metasurfaces for multiuser downlink beamforming in the wave domain," *arXiv preprint arXiv:2309.02687*, 2023.

[10] ——, "Stacked intelligent metasurfaces for efficient holographic MIMO communications in 6G," *IEEE Journal on Selected Areas in Communications*, 2023.

[11] A. Papazafeiropoulos *et al.*, "Achievable rate optimization for stacked intelligent metasurface-assisted holographic MIMO communications," *arXiv preprint arXiv:2402.16415*, 2024.

[12] N. S. Perović *et al.*, "Optimization of the cut-off rate of generalized spatial modulation with transmit precoding," *IEEE Transactions on Communications*, vol. 66, no. 10, pp. 4578–4595, 2018.

[13] ——, "Optimization of RIS-aided MIMO systems via the cutoff rate," *IEEE Wireless Communications Letters*, vol. 10, no. 8, pp. 1692–1696, 2021.

[14] X. Lin *et al.*, "All-optical machine learning using diffractive deep neural networks," *Science*, vol. 361, no. 6406, pp. 1004–1008, 2018.